Spatial distribution and physicochemical properties of respirable volcanic ash from the 16-17 August 2006 Tungurahua eruption (Ecuador), and alveolar epithelium response in-vitro

Julia Eychenne, Lucia Gurioli, David Damby, Corinne Belville, Federica Schiavi, Geoffroy Marceau, Claire Szczepaniak, Christelle Blavignac, Mickaël Laumonier, Emmanuel Gardés, et al.

Spatial distribution and physicochemical properties of respirable volcanic ash from the 16-17 August 2006 Tungurahua eruption (Ecuador), and alveolar epithelium response *in-vitro*

Julia Eychenne[1,2*], Lucia Gurioli[1], David Damby[3], Corinne Belville[2], Federica Schiavi[1], Geoffroy Marceau[2,4], Claire Szczepaniak[5], Christelle Blavignac[5], Mickael Laumonier[1], Emmanuel Gardés[1], Jean-Luc Le Pennec[6,7], Jean-Marie Nedelec[8], Loïc Blanchon[2], Vincent Sapin[2,4]

[1] Université Clermont Auvergne, CNRS, IRD, OPGC, Laboratoire Magmas et Volcans, F-63000 Clermont-Ferrand, France

[2] Université Clermont Auvergne, CNRS, INSERM, Institut de Génétique Reproduction et Développement, F-63000 Clermont-Ferrand, France

[3] U.S. Geological Survey, California Volcano Observatory, Moffett Field, CA, USA

[4] Biochemistry and Molecular Genetic Department, University Hospital, F-63000 Clermont-Ferrand, France

[5] Université Clermont Auvergne, UCA PARTNER, Centre Imagerie Cellulaire Santé, F-63000 Clermont-Ferrand, France

[6] Geo-Ocean, CNRS, Ifremer, UMR6538, F-29280 Plouzané, France

[7] IRD Office for Indonesia & Timor Leste, Jalan Kemang Raya n°4, Jakarta 12730, Indonesia

[8] Université Clermont Auvergne, Clermont Auvergne INP, CNRS, ICCFn, F-63000 Clermont-Ferrand, France

*Corresponding author, julia.eychenne@uca.fr, Laboratoire Magmas et Volcans, Campus Universitaire des Cézeaux, 6 Av. Blaise Pascal, 63178 Aubière Cedex, France

Declaration of conflicts of interest: The authors declare they have nothing to disclose.

Key Points:

- The 16-17 August 2006 Tungurahua eruption produced a high amount of inhalable (12.0-0.04 kg/m^2 of sub-10 µm deposited on the ground) and respirable ash (5.3-0.02 kg/m^2 of sub-4 µm ash deposited on the ground). The

This article has been accepted for publication and undergone full peer review but has not been through the copyediting, typesetting, pagination and proofreading process, which may lead to differences between this version and the Version of Record. Please cite this article as doi: 10.1029/2022GH000680.

abundance and proportion of inhalable and respirable ash vary greatly across the deposit within the first 20 km from the volcano.

- The respirable ash is characteristic of an andesitic magma and no crystalline silica is detected. Morphological features and surface textures are complex and highly variable, with few fibres observed.
- *In-vitro* experiments show that respirable volcanic ash is internalized by A549 cells and processed in the endosomal pathway, causing little cell damage, but resulting in changes in cell morphology and membrane texture. The ash triggers a weak pro-inflammatory response.

ABSTRACT

Tungurahua volcano (Ecuador) intermittently emitted ash between 1999 and 2016, enduringly affecting the surrounding rural area and its population, but its health impact remains poorly documented. We aim to assess the respiratory health hazard posed by the 16-17 August 2006 most intense eruptive phase of Tungurahua. We mapped the spatial distribution of the health-relevant ash size fractions produced by the eruption in the area impacted by ash fallout. We quantified the mineralogy, composition, surface texture, and morphology of a respirable ash sample isolated by aerodynamic separation. We then assessed the cytotoxicity and pro-inflammatory potential of this respirable ash towards lung tissues *in-vitro* using A549 alveolar epithelial cells, by electron microscopy and biochemical assays. The eruption produced a high amount of inhalable and respirable ash (12.0-0.04 kg/m^2 of sub-10 μm and 5.3-0.02 kg/m^2 of sub-4 μm ash deposited). Their abundance and proportion vary greatly across the deposit within the first 20 km from the volcano. The respirable ash is characteristic of an andesitic magma and no crystalline silica is detected. Morphological features and surface textures are complex and highly variable, with few fibres observed. *In-vitro* experiments show that respirable volcanic ash is internalized by A549 cells and processed in the endosomal pathway, causing little cell damage, but resulting in changes in cell morphology and membrane texture. The ash triggers a weak pro-inflammatory response. These data provide the first understanding of the respirable ash hazard near Tungurahua and the extent to which it varies spatially in a fallout deposit.

1 Introduction

Volcanic eruptions are natural phenomena that disperse gaseous species and particles into the atmosphere up to thousands of kilometres away from the source volcano, degrading air quality over vast territories. After the Córdon Caulle eruption in Chile in 2011, for example, increased particulate matter (PM) attributable to volcanic emissions was registered on air quality monitoring stations 1600 km away, in Uruguay (Balsa, Caffera, & Bloomfield, 2016). Closer to active volcanic vents, PM10 concentrations (i.e., PM < 10 μm in size, hence inhalable through the nose and mouth; Brown et al., 2013) exceeding the World Health Organization (WHO) 24-hr mean health safety threshold (50 $\mu g/m^3$) are regularly recorded, such as in Iceland (Carlsen et al., 2015; Thorsteinsson et al., 2012). Today, more than 1 billion people across the globe live within 100 km of active volcanoes, and 225 million within 30 km, many in developing countries (Freire et al., 2019). Communities benefit from fertilized soil and new rock resources, allowing for the emergence of economic activities such as agriculture, quarrying/mining and tourism. These populations also frequently breath an ambient air laden with volcanic particles, not only because volcanic activity can be recurrent for long periods of time (e.g., 1995-2013 Soufrière Hills eruption on the Island of Montserrat; Baxter et al., 2014; Wadge et al., 2014), but also because, after deposition on the ground, volcanic particles are easily remobilized by the wind and human activity (Forte et al., 2018; Jarvis et al., 2020).

The quality of the air we breathe is a major public health concern in the 21st century. In 2019, more than 6 million premature deaths are attributable to fine-particle pollution worldwide (Health Effects Institute, 2020), mainly due to respiratory and cardiovascular diseases. Inhalation of certain mineral dusts, such as asbestos and crystalline silica, is also known to cause acute respiratory diseases and chronic, often irreversible, diseases such as pneumoconioses and cancers (IARC, 2012). The comparison to mineral dust is relevant because explosive volcanic emissions are dominated by particles, called “ash”, which are heterogeneous mixtures of crystalline and amorphous silicates (i.e., mineral species with a chemical composition dominated by Si, and rich in Al, Fe, Mg, Na, Ca, K, and Ti), as well as iron, titanium oxides and sulphate minerals. Volcanic ash is formed by the fragmentation and quenching of magma erupting at the surface of Earth, and the erosion of conduit walls (Cashman & Rust, 2016), and hence have polydisperse size distributions (mm nm), with compositions and physical properties unique to each eruption.

Acute health effects have been documented in exposed populations during several

volcanic eruptions (e.g., 1980 Mount St. Helens, USA; 1995-2013 Montserrat Soufrière Hills, Caribbean; 1995-today Sakurajima, Japan), including the exacerbation of pre-existing chronic lung diseases (Horwell & Baxter, 2006; Stewart et al., 2022). A variable pathogenicity of volcanic ash in the respiratory system has been evidenced by *in-vivo* and *in-vitro* studies. *In-vivo* studies using volcanic ash from the Mount St. Helens and Soufrière Hills eruptions indicated inflammation, fibrosis in the lungs (Green et al., 1981), and granuloma in the lymph (Lee & Richards, 2004). *In-vitro* assays show that volcanic ash can induce an inflammatory response from macrophages and alveolar epithelial cells, despite a limited membranolytic activity (Damby et al., 2016; Horwell et al., 2013; Monick et al., 2013). A recent study using sub-4 μm volcanic ash (hence "respirable"; i.e., capable of entering the gas-exchange region of the lungs) from the Soufrière Hills eruption showed that it can activate the well-established NLRP3 inflammatory pathway (Damby et al., 2018), potentially due to the high crystalline silica component of this sample (about 15 wt.% of cristobalite; Damby et al., 2014). However, the *in-vitro* response to volcanic ash is generally lower than that observed for crystalline silica (Damby et al., 2018), and varies among samples (Damby et al., 2016). The cytotoxic and pro-inflammatory effects of crushed pure phase silicate minerals have proved to be mineral and cell-dependant, with feldspar crystals (a common mineral in volcanic ash) triggering a pro-inflammatory response in macrophages (Grytting et al., 2022; Damby et al., 2018). The physicochemistry of volcanic ash has been studied in relation to the bioreactivity described above, and key properties relevant to toxicity have been identified, namely the particle size distribution, specifically the content in particles finer than 10, 4, 2.5 and 1 μm (Horwell, 2007), the particle morphology (Damby et al., 2013; Horwell et al., 2013), the mineralogical (e.g., crystalline silica content) and chemical composition (Damby et al., 2017; Horwell et al., 2013), and the oxidative potential of the particles (Horwell et al., 2003).

Despite this knowledge, anticipating the health hazard at a volcano where no health-focused studies have been carried out remains a challenge. This is due to the high variability of volcanic ash from one volcanic eruption to another, which limits the extent to which the lessons learnt in one volcanic environment can be transferred to another (Stewart et al., 2022). The present work aims to characterize health-relevant properties of the volcanic ash from the 1999-2016 Tungurahua eruption, in Ecuador, and to assess the bioreactivity *in-vitro* using alveolar epithelial cells. This long-lasting eruption of

Tungurahua has strongly and enduringly affected the surrounding rural area and its population (Few, Armijos, & Barclay, 2017), due to the volcanic emissions, and in particular the large amount of volcanic ash, recurrently dispersed in the environment by explosive episodes (Bustillos et al., 2016; Eychenne et al., 2012; Le Pennec et al., 2012). The resuspension of the ash-rich, powdery soils created during the nearly two decades of eruption means that some of the hazards and impacts from this eruption persist even today. Tungurahua is ranked as the most hazardous volcano in South America (Guimarães et al., 2021), due to the high recurrence rate of high-intensity explosive eruptions, but little is documented about the impact of the eruptions on population health. Studying the health hazard presented by the activity of this volcano is thus of the utmost relevance. After describing the spatial distribution of inhalable and respirable volcanic ash dispersed in the environment during the most intense explosive phase of the eruption, which occurred on 16-17 August 2006, we describe the physicochemical properties of the respirable ash, and assay the alveolar epithelium response to this ash *in-vitro*.

1.1 Volcanological context at Tungurahua

The 5023 m-high Tungurahua volcano is located in the southern part of the eastern Andean Cordillera, at the limit with the Amazon basin (Fig. 1a,b). This stratovolcano began a new explosive eruption at the end of 1999 after 80 years of repose (Le Pennec et al., 2012). The eruption lasted until 2016 and alternated phases of repose and low to high intensity explosive activity, with 2 to 3 phases of activity per year on average (Fig. 1c; Hidalgo et al., 2015; Muller et al., 2018). The magma emitted was andesitic in composition (about 58 wt.% of SiO_2). During phases of activity, particle and gas rich volcanic plumes rose 1 to 18 km above the crater and, due to the prevailing east-to-west winds, dispersed volcanic ash on the western and, more rarely, the southern and northern areas (B. Bernard, 2013; Bustillos et al., 2016; Eychenne et al., 2012; Le Pennec et al., 2012). The volcano slopes were also regularly affected by pyroclastic density currents (PDCs), which are mixtures of hot fragmented volcanic material and gas that flow down the topography (J. Bernard et al., 2014), depositing ash.

The most explosive phase of activity (paroxysmal phase) occurred on 16-17 August 2006 (local time), lasting about 4 hours, and produced 100.8 ± 21.1 x 10^9 kg of fragmented material (J. Bernard et al., 2016). About a quarter of this material dispersed in the western direction from a volcanic plume that rose 16-18 km above the crater, and deposited particles up to 60 km away from the volcano in the northern direction and to distances

greater than 100 km towards the west (Eychenne et al., 2012). A further half of the fragmented material was transported in PDCs that covered the western slope of the volcano (J. Bernard et al., 2016). Concomitant generation of co-PDC plumes occurred, a process by which ash roughly finer than 100 μm in size, escapes PDCs by elutriation during flow propagation, which generates ash clouds that rise and disperse through the atmosphere (Engwell & Eychenne, 2016). The co-PDC plumes dispersed towards the west, in the same direction as the crater-derived plume due to the prevailing winds, leading to a remarkable enrichment in sub-100 μm ash in the deposit resulting from particle fallout on the ground (Eychenne et al., 2012). During the weeks following the 16-17 August 2006 eruptive phase, this fallout deposit was surveyed by field campaigns, and sampled at the locations represented in Fig. 1b. The total mass of particles deposited per unit area (MpUA) was measured and the full grain size distribution of each sample was determined in the laboratory (Eychenne et al., 2012).

1.2 Background on the Tungurahua social-ecological system

About 20,000 people live in the small tourist town of Baños at the northern foot of Tungurahua volcano. The lower northwest, west, and southwest slopes of the volcano, as well as the western plateau of Quero, are farmed and populated by small rural communities (Fig. 1b, Fig. 2a). A total of 32,000 people live within 15 km of the volcano (Few, Armijos, & Barclay, 2017). The recurrent eruptive activity between 1999 and 2016 produced powdery deposits (Fig. 2b), which still cover the topography in places around Tungurahua and are continually remobilized by the wind and human activity. They constitute the soils on which human activity has carried on since 1999. Indeed, the local populations were evacuated to nearby areas not affected by the volcanic activity in 1999, but settled back into their homes as soon as 2000 (Tobin & Whiteford, 2002; Whiteford & Tobin, 2004).

Over the next 20 years, the local people learned how to live with the volcanic risk. They developed a unique crisis management network, based on the close interaction between the scientists in charge of monitoring the volcano and each community (Mothes et al., 2015; Stone et al., 2014). Thanks to voluntary and timely evacuations prior to each of the high intensity explosive phases, the communities were able to remain on their lands throughout the duration of the eruption with few fatalities (Armijos et al., 2017; Barclay et al., 2019). The populations coped with the recurring environmental changes caused by the eruptive activity by implementing adaptation strategies that allowed them to

minimize the impacts on agriculture (Armijos et al., 2017; Few et al., 2017). They selected crops resistant to volcanic ash and developed cultivation methods that minimized their vulnerability (Few et al., 2017). After each major eruptive phase, the crops, meadows, and farms were rapidly cleaned and reclaimed for agriculture. For all of these reasons, Tungurahua is an example of a resilient volcanic social-ecological system. But this remarkable resilience has promoted a prolonged exposure of the population to volcanic PM, exacerbated by the outdoor occupational activity of most people, farming being the principal occupation of 60 to 70% of adults living in the rural surroundings of Tungurahua (Few et al., 2017). During the 1995-2013 Soufrière Hills eruption on the Island of Montserrat, comprehensive surveys of personal exposure demonstrated that outdoor workers were the most exposed to airborne volcanic ash (Searl, Nicholl, & Baxter, 2002). This situation is the motivation for determining the respiratory hazard of the volcanic ash from Tungurahua.

1.3 State of knowledge on the health impact of the Tungurahua eruption

Scarce data on the health impact of the long-lasting Tungurahua eruption are available. Analysis of health records up to 2001 from local health care centres and qualitative surveys in the communities surrounding the volcano in 2001 demonstrated an increase in acute respiratory infections and self-reported respiratory problems in the year following the start of the eruption (Tobin & Whiteford, 2004). Respiratory problems, as well as skin and digestive problems (related to eating and drinking food and water contaminated by volcanic ash), were reported in 2010, after 10 years of volcanic activity, by healthcare professionals working in local health centres (Sword-Daniels et al., 2011). Despite these observations, no public health mitigation strategies were implemented to monitor and minimize the impacts of the volcanic eruption on the population. In addition, despite several volcanological studies describing the physicochemistry of the volcanic particles produced by this eruption (Eychenne et al., 2013; Eychenne et al., 2012; Leibrandt & Le Pennec, 2015; Samaniego et al., 2011; Wright et al., 2012), the respirable ash fraction has never been characterized, neither has its bioreactivity been studied. This work aims at filling these stark gaps in knowledge.

2 Material and methods

2.1 Mapping the inhalable volcanic ash fractions deposited

Using the field samples and grainsize data presented in Eychenne et al. (2012) and summarized in section 1.1, the weight proportions of particles in different fractions of the

inhalable size range (< 10, < 4, < 2.5, < 1 μm) for each fallout sample (Fig. 1b) were quantified and converted to MpUA (using the total MpUA data of Eychenne et al., 2012). These MpUA data for each inhalable volcanic ash fraction were used (1) to quantify their decay rate away from the volcano and (2) to build maps of their distribution on the ground in the surrounding environment of the volcano by interpolating manually between sampled locations. Note that in Eychenne et al. (2012), the full grain size distribution of each sample was determined by sieving the particles coarser than 63 μm at half phi intervals (where phi=-$\log_2$ (grain diameter in mm)), and by laser diffraction measurements of the particles finer than 90 μm using a Malvern Mastersizer 2000 (absorption coefficient of 0.1, refractive index of 1.53).

2.2 Volcanic sample preparation and characterization

2.2.1 Isolation of a respirable ash sample

We selected one key fallout sample (sample F2) from the 16-17 August 2006 eruptive phase, collected on 14 September 2006 in Pillate (Fig. 1b), located 7.9 km away from the eruptive vent along the main axis of plume dispersion and PDC propagation. A respirable fraction (sizes < 4 μm) was physically isolated from this bulk sample using an aerodynamic separation method set up at the USGS California Volcano Observatory, given that sieving to such small grain size is not feasible. In short, the bulk sample was sucked at a steady flow rate equivalent to the terminal settling velocity of 4 μm particles, and allowed to fall in a settling chamber to remove aggregates and particles coarser than about 4 μm. The respirable ash was then collected on a filter holder downstream of the settling chamber (Tomašek et al., 2016). The grain size distribution of the isolated respirable ash was measured by laser diffraction using a Malvern Mastersizer 3000 at *Institut de Chimie de Clermont-Ferrand*, France (absorption coefficient of 0.1, refractive index of 1.63).

2.2.2 Physicochemical characterization of the respirable ash

The mineralogy of the respirable ash was assessed by Raman spectroscopy at *Laboratoire Magmas et Volcans* (LMV, Clermont-Ferrand, France) on unpolished mounts of grains dispersed on carbon sticky tape, and on polished mounts of grains laid in a light-cured universal micro hybrid composite (dental paste Kentfil+). The spectra were collected on individual grains using an InVia confocal Raman micro-spectrometer (*Renishaw*) and equipped with a 532 nm diode laser (200 mW output power), a Peltier-cooled CCD detector of 1040 × 256 pixels, a motorised XYZ stage, and a Leica DM 2500 M optical

microscope. The scattered light was collected using a back-scattered geometry. The analytical settings used were a laser power at the grain surface between 0.1 and 1 mW, an acquisition time between 15 and 60 s, a grating of 2400 grooves mm^{-1}, a 100x microscope objective and a 20-µm slit aperture (high confocality setting). The wavelength was systematically calibrated prior to analysis, based on the 520.5 cm^{-1} peak of Si. Spectra were recorded in the wavenumber range 60-1410 cm^{-1} (vibrational frequencies of mineral phases and alumino-silicate network domain of glasses), and occasionally in the 2800-3900 cm^{-1} range to check for H_2O and OH molecules. Individual spectra were interpreted in terms of phase (mineral, glass or mixture of mineral(s) and glass) by fitting the main peaks or bands, using reference libraries (RRUFF™ project and Thermo Fisher Grams Spectral ID®) and publications (Frezzotti, Tecce, & Casagli, 2012; Schiavi et al., 2018). The proportion of each of the identified phases in the sample was quantified by acquiring a total of 133 spectra on individual grains, thereby determining the mineralogical assemblage of the respirable ash sample.

The morphology, surface texture and composition of the respirable ash were assessed on a *Helios 5* (*ThermoFisher Scientific*) scanning electron microscope coupled with a focused ion beam (Xe plasma; FIB-SEM) at LMV, France, on unpolished mounts of grains dispersed on polycarbonate membranes, stuck on carbon sticky tape and carbon coated. High-resolution images were acquired in secondary electron (SE) and backscattered electron (BSE) modes using electron acceleration voltages of 2 to 5 kV, a current of 50 pA and a 5.0 mm working distance. Elemental composition was measured by energy dispersive X-ray spectroscopy (EDS) with a 60 mm^2 annular *FLATQUAD* detector (*Bruker*) with beam conditions of 10 kV / 0.8 nA and a 13 mm working distance.

2.3 In-vitro bioreactivity assays

2.3.1 Cell culture and treatment with respirable volcanic ash

Immortalized human type II alveolar epithelial cells of the A549 cell line were treated with the isolated respirable volcanic ash sample from Tungurahua volcano, obtained using the aerodynamic separation method presented in section 2.2.1. The cells were maintained in culture at 37 °C in a 5% CO_2 environment in DMEM growth media (Gibco, Thermo Fisher Scientific, Grand Island, USA) supplemented with 10% FBS (Eurobio Scientific, Les Ulis, France), 4 mM L-glutamine (Gibco), and 100 U/ml penicillin, 0.1 mg/ml streptomycin, 0.25 µg/ml amphotericin B (Eurobio Scientific). Twenty-four hours before treatment, cells were trypsinized using a 0.25% solution (Gibco), seeded at a density of 1 x 10^6

cells/well in 1 ml of complete medium in 6-well plates and allowed to adhere overnight. Cells were treated in quadruplet for either 6 or 24 hours, with suspensions of the Tungurahua respirable volcanic ash or a positive particle control (Min-U-Sil quartz < 10 µm, which is a benchmark sample well-known for its cytotoxicity and inflammatory activity; Geys, Nemery, & Hoet, 2010). Particles were suspended at 250 and 1000 µg/ml (based on published dose-response curves for volcanic particles; Damby et al., 2016) in serum-free DMEM media and vortexed prior to cell treatment with 1 ml of suspension. These particle concentrations are equivalent to 26 and 105 µg/cm^2 in 6-well plates. Experiments were repeated 6 times.

After 6 or 24 hours of treatment: (1) culture medium was removed from each well and centrifuged at 13,000 rpm for 10 minutes in 1.5 ml Eppendorf tubes to remove cell debris or remaining particles, and 850 µl of supernatant was then collected and stored at -80 °C until further analyses; (2) cells were washed 3 times in 1 ml of PBS 1x (Eurobio Scientific), then scratched from the bottom of the wells and centrifuged at 13,000 rpm for 10 minutes in 1.5 ml Eppendorf tubes and stored at -20 °C after removing the supernatant.

Equivalent experiments in terms of exposure durations and doses were performed in duplicate by seeding 5 x 10^5 cells/well in 12 well plates on Thermanox™ coverslips (Thermo Fisher Scientific, Grand Island, USA) for subsequent preparation and imaging by Transmission Electron Microscopy (TEM) and Field Emission Gun (FEG)-SEM.

2.3.2 Cytotoxicity assay

Cytolysis was assessed by lactate dehydrogenase (LDH) assay in merged culture media of 2 replicates of the 6 independent experiments (leaving duplicates for each experiment). Activity of LDH was quantified with an automated enzymatic assay (Vista, Siemens Health Diagnosis, Paris, France), following the manufacturer's recommendations.

2.3.3 Assessment of the pro-inflammatory response

The pro-inflammatory response was assessed by quantifying the cytokines interleukin (IL)-6, IL-8, IL-1β and tumor necrosis factor (TNF)-α, at gene transcript and protein levels. Transcript quantification was measured by real-time quantitative Reverse Transcription Polymerase Chain Reaction (RT-qPCR) using the merged cell pellets from two replicates (leaving duplicates for each experiment) in order to recover enough ribonucleic acid (RNA) for each studied condition. Total RNA extraction was performed using the NucleoSpin RNA Mini kit (Macherey-Nagel GmbH, Düren, Germany) according to the manufacturer's protocol. RNA concentrations in cell extracts were measured with a DS-

11FX spectrophotometer (DeNovix Inc, Wilmington, USA). Complementary deoxyribonucleic acid (cDNA) was synthesized by reverse transcription on 1 µg of RNA using the Superscript IV First-Strand Synthesis system (Invitrogen, Thermo Fisher Scientific, Grand Island, USA), following the manufacturer's instructions. PCR experiments were performed using specific oligonucleotides (Table 1). RT-qPCR was performed using LightCycler® 480 SYBR Green I Master (Roche, Meylan, France). Transcript quantification was performed in duplicate on four independent experiments. Quantification of amplified transcripts was assessed using standard curves, and gene expression was then normalized to the geometric mean of the housekeeping human genes *RPLP0* (36B4) and *RPS17* (acidic ribosomal phosphoprotein P0 and ribosomal protein S17, respectively), as recommended by the MIQE guidelines (Bustin et al., 2009).

Cytokine release into the culture media was quantified using automated multiplex immunoassays on Ella™ (San Jose, CA, USA), following the manufacturer's instructions, on the 4 merged replicates of the 6 independent experiments. Total protein concentrations in the samples were measured using the BCA Protein Assay Kit (Pierce, Thermo Fisher Scientific, Grand Island, USA), and results used to normalize the cytokine concentrations.

2.3.4 Statistical analysis

Statistical analysis was performed using GraphPad PRISM software (San Diego, CA, USA). Results for each condition were compared using the Kruskal-Wallis one-way analysis of variance with Dunn's post-test. Differences between conditions were considered significant at $p \leq 0.05$.

2.3.5 Particle-cell interactions imaging

After 6 or 24 hours of treatment, the cells grown on Thermanox™ coverslips were fixed overnight at 4 °C with 1.6% glutaraldehyde in 0.2 M sodium cacodylate buffer, pH 7.4.

For FEG-SEM analyses, samples were then washed for 30 minutes in the same sodium cacodylate buffer (0.2 M, pH 7.4) and post-fixed for 1 hour with 1% osmium tetroxide in the same buffer. After rinsing for 20 minutes in distilled water, dehydration by graded ethanol was performed at 25, 50, 70, 95 and 100% ethanol concentrations (10 minutes at each concentration), to finish in hexamethyldisilazane (HMDS) for 10 minutes. Samples were mounted on stubs using adhesive carbon tabs and coated with chrome (Quorum Q150 TES). Observations were carried out using a Regulus 8230 FEG-SEM (Hitachi, Japan) at 1 and 2 kV with a SE detector and a 13 mm working distance. Elemental microanalysis

was performed with an Ultim Max 170 mm^2 EDS system from Oxford Instrument at 10 kV and a 15 mm working distance.

For TEM analyses, samples were washed three times in sodium cacodylate buffer (0.2 M, pH 7.4) then post-fixed for 1 hour with 1% osmium tetroxide and washed three times (10 min per wash) in this buffer. Samples were dehydrated in a graded ethanol solution (25, 50, 70, 95 and 100% ethanol). They were then infiltrated for 1 hour with each of the following mixtures: (1) 2 volumes of ethanol 100% with 1 volume of EPON resin, (2) 1 volume of ethanol 100% with 1 volume of EPON resin, and (3) 1 volume of ethanol 100% with 2 volumes of EPON resin. Finally, samples were infiltrated with resin overnight at room temperature and polymerized for 2 days in a 60 °C oven. Ultrathin sections (70 nm thick) were cut in the samples using a UC7 ultramicrotome (Leica, Wetzlar, Germany) and stained with uranyl acetate and lead citrate. Note that the hardness contrast between the mineral particles (ash and quartz) and the cells and resin led to unpreventable tears in some sections. The sample sections were imaged at 80 kV with a TEM H-7650 (Hitachi, Japan) and a Hamamatsu AMT40 camera.

Electron microscopy preparations and analyses were all performed at the *Centre Imagerie Cellulaire Santé* (Clermont-Ferrand, France). All the chemical products were from Electron Microscopy Science, and distributed in France by Delta Microscopies.

3 Results

3.1 Spatial distribution of the inhalable volcanic ash fractions

Within less than 20 km from the volcano, the fallout deposit from the 16-17 August 2006 paroxysmal phase of the Tungurahua eruption was rich in inhalable particles, with sub-10 µm ash constituting 12.0 to 1.5 wt.% of the deposit, sub-4 µm 6.0 to 0.6 wt.%, sub-2.5 µm 4.8 to 0.5 wt.% and sub-1 µm 2.4 to 0.3 wt.% (Table 2). When normalized to the total mass of particles deposited, these values correspond to 12.0 to 0.04 kg/m^2 of sub-10 µm ash deposited, 5.3 to 0.02 kg/m^2 of sub-4 µm, 4.1 to 0.01 kg/m^2 of sub-2.5 µm and 1.9 to 0.01 kg/m^2 of sub-1 µm (Table 2).

A high spatial variability is observable, with a general decrease with distance from vent of the amount of inhalable ash deposited (Fig. 3). Two decay trends can be noted: (i) a main, steep trend (shaded areas on Fig. 3a,b) corresponding to the variations along the depositional axis oriented west-northwest, where the highest values of MpUA are found for all the inhalable ash fractions (Fig. 3d-g); (ii) a secondary, shallower trend (open symbols on Fig. 3b) corresponding to areas north and south of the depositional axis,

where lower values of MpUA are found but spread across a wider spatial area (Fig. 3d-g). Interestingly, the wt.% and MpUA decay trends reveal some differences. The proportions and MpuA of the inhalable ash fractions both decrease with distance from vent (more slowly for the proportions than the MpUA values, Fig. 3a,b). An increase in wt.% with distance is notable between 15 and 20 km from vent within the secondary trends of all the inhalable ash fractions (Fig. 3a), which is not discernible within the MpUA variations (Fig. 3b). The wt.% of the sub-63 μm ash also show a general decrease along the axis and an increase between 15 and 20 km from vent in the off-axis samples (Fig. 3c). The MpUA variations of the inhalable ash fractions mimic the mass variations in the total deposit and in the ash fraction finer than 63 μm (Fig. 3c), with a break-in-slope around 10 km from vent in the decay trend (Fig. 3b,c).

3.2 Physicochemical properties of the respirable ash

The grain size distribution (volume %) of the respirable ash sample isolated from sample F2 by aerodynamic separation has a median diameter of 2.5 μm, and a 10^{th} and 90^{th} percentile of 1.1 and 5.9 μm, respectively (Fig. 4a). With 75 vol.% of the sample finer than 4 μm, this ash sample is confirmed as respirable.

The mineralogical phases identified by Raman spectroscopy in the above-mentioned respirable ash sample are: (1) andesitic and rhyolitic glass, (2) crystals of feldspars (plagioclase and sanidine), clinopyroxene (augite and pigeonite), and orthopyroxene (hypersthene), (3) iron and titanium oxides (magnetite, hematite and anatase), and (4) potassium aluminium sulfates (alunite) (Fig. 4b,c and Table 3). SEM-EDS analyses confirm the Raman data (see chemical maps in Fig. 5). The proportions in the respirable ash sample of the different phases mentioned above, as well as their standard chemical compositions, are given in Table 3. Additional accessory phases (less than 1% of the phases) include rutile, olivine, and carbonaceous matter. No crystalline silica was detected by Raman spectroscopy.

The morphology and surface texture of the particles imaged by SEM are highly variable and dependent on particle composition (Fig. 5). Glass fragments (K-rich phases on EDS maps, Fig. 5k-n) tend to have concave flat shapes and smooth surfaces, which sometimes are remnant vesicle walls (Fig. 5a,c,d,f,h,i). Plagioclase (Al-rich phases on EDS maps, Fig. 5k-n) and pyroxene (Mg-rich on EDS maps, Fig. 5k-n) crystals are either euhedral, free fragments, or included in glass (Fig. 5b,c,g,h). Clinopyroxene (Ca-rich phases on EDS maps, Fig. 5m) and orthopyroxene are sometime observed associated (Fig. 5m). Crystal sizes

vary between > 10 μm in length (euhedral) to < 1 μm (Fig. 5h). Pyroxene crystals tend to be smaller than plagioclase ones. Fractured surfaces are prevalent, both on crystals (Fig. 5b,g) and glass particles. Many Fe-Ti oxides are observed as free < 500 nm particles, or as nanolites in andesitic glass, creating a granular surface (Fig. 5e,j,l,n). The sulfate salts (alunite) are found as free particles that are ~3 μm to a few 100s nm in size (Fig. 5l,n). All micrometer-sized particles are covered with smaller particles that are up to a few 100s nm in size. These small particles are either fragments from the andesitic and rhyolitic magmatic assemblage (e.g., glass, pyroxenes, plagioclases, Fe-Ti oxides), or sulfate salts, also visible as small nanometer-sized features at higher magnification on glassy surfaces. Very few fibre-like particles are observed.

3.3 In-vitro reactivity of the respirable ash

Treatment of A549 cells with the respirable volcanic ash and quartz particles leads to changes in cell morphology, membrane texture, and intracellular characteristics (Fig. 6). FEG-SEM images of the A549 cells show that untreated cells create layers of joint cells with spread out shapes (Fig. 6a-d). The surfaces of the membrane display elongated filaments. After 24 hours, slightly retracted cell morphologies can be noted (Fig. 6c,d). Cells treated with respirable volcanic ash have more retracted shapes than untreated cells, and cell junctions are lost (Fig. 6e-g). After 24 hours of treatment, the membrane's surface appears rough and micro-perforated (Fig. 6g,h). No major differences can be observed between the 250 and 1000 μg/ml doses (Fig. S1 in Supplemental Material). Particles are observed lying on the surface of the cells (Fig. 6f,g) or entangled in their membrane, with filaments embedding the particles (Fig. 6h). Cells treated with quartz particles are entirely retracted with sphere-like morphologies as early as 6 hours after treatment (Fig. 6i,j). Particles are observed as agglomerates on the cells' surfaces (Fig. 6k) or entangled in the membrane (Fig. 6l).

TEM images of A549 cell sections show that untreated cells form a layer with tight junctions and have spread out shapes after 6 and 24 hours of culture in serum-free medium (Fig. 6m,o). Round nuclei containing chromatin can be observed (Fig. 6m-o), as well as numerous organelles in the cytoplasm, including mitochondria and lamellar bodies, the latest producing the pulmonary surfactant in type II epithelial cells (Fig. 6m-p). Many autophagosomes/autophagolysosomes are also present, potentially due to the established upregulated autophagosomal activity of the A549 cell line. Cells treated with respirable volcanic ash contain internalized particles in the cytoplasm, in

autophagosomes/autophagolysosomes (where lamellar bodies and mitochondria are often present, too) or multivesicular bodies (Fig. 6q-t). An attempt of endocytosis is also observed at the membrane (Fig. 6r). Despite this endosomal activity, the cells treated with respirable volcanic ash for 6 and 24 hours preserved their overall integrity (Fig. 6q-t). Cells treated with quartz also contain internalized particles, autophagosomes/autophagolysosomes and microvesicular bodies (Fig. 6u-x). As soon as 6 hours after treatment, cells have retracted shapes and small lysis vacuoles in the cytoplasm (Fig. 6u,v). After 24 hours of treatment, the cells have lost their integrity, with large lysis vacuoles in the cytoplasm, and disintegrated membranes and nuclei (Fig. 6w,x). Both cells treated with respirable volcanic ash and quartz particles contain numerous microvesicular bodies after 24 hours of treatment, which are filled with dark spots (Fig. 6t,w).

LDH activity indicates little effect of the respirable volcanic ash treatment on A549 cell viability (Fig. 7a). Conversely, the quartz treatment triggered a high LDH release, which increased after 24 hours of exposure (Fig. 7a), indicative of time-enhanced cytotoxicity, in agreement with the known toxicity of Min-U-Sil quartz (Geys et al., 2010).

The pro-inflammatory response of A549 cells was particle, cytokine, time and dose dependent (Fig. 7b,c). At gene level, a significant upregulation of *IL6* and *TNF* is triggered by the quartz positive control as early as 6 hours after treatment (Fig. 7b). The quartz treatment also augments the expression of *IL8* after 6 hours, but not the expression of *IL1B* (Fig. 7b). After 24 hours of treatment, only the upregulation of *IL6* by quartz is still significant (Fig. 7b). No significant upregulation of *IL6*, *IL8*, *TNF* and *IL1B* is detectable after 6 and 24 hours of respirable volcanic ash treatment (Fig. 7b). At protein level, IL-6, IL-8 and TNF-α release was clearly triggered by 6 and 24 hours of quartz treatment (Fig. 7c), while IL-1β production was not triggered by the quartz insult (Fig. 7b,c). A dose- and time-enhanced IL-6 production due to the respirable volcanic ash treatment is observable at the protein level, with a significant difference compared to untreated cells for the high ash dose (1000 µg/ml, or 105 µg/cm^2) at 24 hours (Fig. 7c). Ash-triggered IL-8 production can also be noted at protein level, but not significantly different from untreated cells. No production of TNF-α or IL-1β occurred after 6 or 24 hours of respirable volcanic ash exposure (Fig. 7c).

4 Discussion

4.1 Inhalable ash spatial distribution and implications for exposure

The fallout deposit from the paroxysmal explosive phase of 16-17 August 2006 is rich in inhalable and respirable volcanic ash in the studied area (up to 20 km from vent, Fig. 3 and Table 2). This mirrors the remarkably high content of sub-63 μm ash previously highlighted in this deposit and explained by the co-PDC ash contribution (Eychenne et al., 2012). We observe a decrease in the sub-63 μm ash proportions away from vent along the deposit axis (Fig. 3c), and a similar decreasing trend in the proportions of the inhalable ash fractions with distance from vent (Fig. 3a). These trends are counter-intuitive given that all fallout deposits show a decrease in grainsize with distance from vent (Eychenne & Engwell, 2022; Fisher, 1964), which should lead to an increase in the proportions of sub-63 μm and sub-10 μm ash with distance. These unexpected trends can be explained by the contribution of co-PDC ash, which decreases with the distance to the PDCs, as demonstrated in Eychenne et al. (2012). At Tungurahua volcano, due to the topography, the PDCs propagate towards the west and always stop in the deep canyon of the Chambo River where they remain confined to the east of the Quero plateau (Fig. 1b). These findings indicate that the high amount of inhalable and respirable ash found in the fallout deposit of the August 2006 paroxysmal phase is attributable to the PDC activity.

Enrichment of fallout deposits by ash from PDCs is not restricted to the case of the August 2006 Tungurahua eruptive phase; it is a frequent process documented elsewhere (e.g., May 18, 1980 Mount St. Helens eruption (Eychenne et al., 2015), 1995-2013 Soufrière Hills eruption (Bonadonna et al., 2002)). In fact, many eruptions from intermediate to high explosivity produce ash plumes and PDCs concomitantly (J. Bernard et al., 2016). Particles transported in PDCs have undergone a secondary fragmentation process (the primary fragmentation being that of the magma in the volcanic conduit) by comminution of bigger grains (grain-to-grain abrasion) during their transport (J. Bernard & Le Pennec, 2016; Buckland et al., 2018; Hornby et al., 2020). Understanding the origin of the inhalable ash fractions is thus essential, because secondary fragmentation could affect the size, morphology and surface properties of the grains, which are relevant for toxicity.

Importantly, this work highlights a large spatial variability in inhalable ash contents across the fallout deposit (Fig. 3). The variation trends are different depending on whether the inhalable ash content is expressed as proportion or as MpUA. The proportions of the inhalable ash fractions decrease away from vent along the depositional axis, and increase away from vent off-axis. The main MpUA decay trends of the inhalable fractions along the deposit axis are characteristic of fallout deposits, with a break-in-slope

around 10 km from vent (notable in the total and sub-63 μm MpUA trends, too; Fig. 3c), reflecting a well-known change in particle settling behaviour from volcanic plumes (Bonadonna, Ernst, & Sparks, 1998; Eychenne & Engwell, 2022). Both the proportion and MpUA metrics being based on the deposit-record, they are not directly representative of what people actually breathe (Searl et al., 2002). Rather, they represent available inhalable and respirable material found in the air during the eruption, and on the ground after particle deposition where they are susceptible to resuspension.

Our results establish MpUA of the inhalable ash fractions as a valuable metric for quantifying available material for inhalation and can support assessment of the respiratory health hazard. Whereas proportions give a relative representation of available ash size fractions relevant for respiratory health, they do not account for the uneven absolute amount of volcanic particles distributed spatially (Fig. 3a). Our work also demonstrates that accounting for the spatial variability in inhalable and respirable ash content is critical for hazard assessment, given that, in our dataset, MpUA values for sub-10 and sub-4 μm ash vary by one order of magnitude within 20 km from the source (Fig. 3b-f). Mapping of the sub-10 μm ash fractions has never been achieved by the volcanology community, which rather focuses on coarser grainsize fractions, more relevant to understanding volcanological phenomena. This makes comparing the inhalable and respirable ash content of the fallout deposit from the 2006 Tungurahua eruption to deposits from other eruptions challenging.

These results have important implications for population exposure around Tungurahua volcano. During the August 2006 eruptive phase, the highest amount of inhalable and respirable ash (up to 12.0 and 5.3 kg/m^2 of sub-10 and sub-4μm ash, respectively; Table 2) were deposited in the agricultural area of the Quero plateau, where all of the land is farmed and many small villages are located (Fig. 1b). During this eruption, only populations east of the Chambo River (living on the lower flanks of the edifice; Fig. 1b) were evacuated, and even they eventually settled back on their lands (Armijos et al., 2017). The farmers continued to work on their pastures and crops despite the material deposited. The 2006 phase is only one among dozens that dispersed volcanic ash in the western and, more rarely, the southern and northern areas surrounding Tungurahua over the course of the 1999-2016 eruption (B. Bernard, 2013; Bustillos et al., 2016; Le Pennec et al., 2012) This means that the amount of inhalable and respirable ash determined in this work represents a minimum estimate. Given that most populations around

Tungurahua are outdoor workers (Armijos et al., 2017; Barclay et al., 2019; Few et al., 2017), and that housing and vehicles are permeable due to the mild regional weather, people have a high risk of respiratory exposure to PM in their environment. A similar elevated risk resulting from socio-economic and environmental factors was highlighted during the Soufrière Hills eruption on the island of Montserrat (Baxter et al., 2014; Searl et al., 2002).

An important parameter to assess population exposure to volcanic PM is how long ash particles remain available for resuspension in the environment. Some volcanic ash deposits are still remobilised more than a hundred years after eruption, with large regional impacts, e.g., deposits from the 1912 Novarupta eruption in the Katmai region of Alaska (Hadley, Hufford, & Simpson, 2004). Timescales of unconsolidated volcanic ash deposit preservation depend on several environmental factors that result in their incorporations and transformation to soils. They include climate, with soils developing slower in drier environments (Forte et al., 2018; Jarvis et al., 2020), and the nature of the vegetation cover, whereby ash deposits stabilize more efficiently in vegetated environments (Cutler et al., 2016). Population exposure to volcanic PM after eruptions is thus likely to be highly variable spatially, and its assessment requires an understanding of the spatial distribution of the ash size fractions relevant for respiratory health within the initial fallout deposit, and of the spatio-temporal variations of the environmental parameters described above.

4.2 Physicochemical properties of the respirable volcanic ash

The mineralogical assemblage of the isolated respirable ash sample from the 16-17 August 2006 fallout deposit is characteristic of an andesitic magma (andesitic glass, plagioclase, pyroxene, and Fe-Ti oxides) and is consistent with petrological data acquired on lapilli and bombs from the same eruption (Samaniego et al., 2011). The other identified phases (Fig. 4, Table 3) are also consistent with the eruptive dynamics of the 2006 Tungurahua eruption: (1) the rhyolitic glass and the sanidine crystals originate from the eruption of a more differentiated magma pocket, as previously demonstrated (Samaniego et al., 2011), which only represents 0.4 vol.% of the fallout deposit (Eychenne et al., 2013), and (2) alunite probably originates from the condensation of volcanic gas on ash particles during their transport in the eruption plume and atmosphere, a well know phenomenon during explosive volcanic eruptions (Delmelle et al., 2007; Moune, Gauthier, & Delmelle, 2010). The origin of the carbonaceous matter is unknown, but can be due to burning

vegetation or entrainment of organic material during the eruption. Observation of carbonaceous matter in this respirable volcanic ash further substantiates that people are rarely exposed to volcanic PM alone (Tomašek et al., 2021a).

The morphology and surface texture of the respirable ash (Fig. 5) is highly variable and phase dependant. Crystals have the highest surface roughness, and crystal fragments appear not to be broken along grain boundaries (e.g., Fig. 5m). Fractured surfaces are observed on both crystals and glass, and all particle types are covered with sub-1 μm adhering particles, which are predominantly chips of the magmatic particles and, more rarely, sulfates (Fig. 5k-n). Freshly fractured surfaces in pure-phase silicate minerals have been shown to be more reactive (e.g., generating reactive oxygen species, disrupting cell membranes; Hendrix et al., 2019; Pavan et al., 2022), and new-surface generation of volcanic ash can also increase reactivity (hydroxyl radical production; Damby et al., 2017). The hazard associated with the fractured surfaces observed here is challenging to assess, given that how reactivity changes with time is unknown, and that exposure long after ash generation and initial fracturing is expected in the Tungurahua volcanic environment.

4.3 Bioreactivity and implications for the respiratory hazard

Contrary to quartz, exposure to the Tungurahua respirable ash is weakly cytotoxic towards A549 alveolar epithelial type II cells, as demonstrated by the LDH assay (Fig. 7a) and the TEM and SEM imaging (Fig. 6). The SEM images (Fig. 6e-h) demonstrate a change in cell morphology and membrane texture after exposure to respirable ash, which suggests that the cells start undergoing some suffering, and a potential phenotype change. TEM images demonstrate that the respirable ash particles are internalized by the cells and processed in the endosomal pathway. The fate of these particles after 24 hours is yet to be determined. Dissolution of ash in artificial lysosomal fluid, intended to reflect biodurability in intracellular compartments, or simulated lung fluid is expected over timescales of months to decades, and is dependent on the glass and mineral assemblage (Damby, 2012). The dissolution time of a 1 μm diameter olivine particle, for example, has been demonstrated to be 24 years in simulated lung fluid (Hendrix et al., 2021). If particles are not efficiently digested, they will remain in the lungs or be translocated, such as to the lymphatic system, as evidenced *in-vivo* via instillation of volcanic ash from the Montserrat Soufrière Hills eruption (Lee & Richards, 2004), where persistence or continued dissolution may result in sustained inflammation or continuous release of ions into

solution (Tomašek et al., 2021b). Element release, specifically release of highly bioaccessible elements such as metals (e.g., Cu, Zn, Pb; Sauzéat et al., 2022), can be a mechanism for long-term deregulation of the organism and disease (Sauzéat et al., 2018). Despite being a widely used model in toxicology, few studies have explored the response of A549 alveolar epithelial type II cells to respirable volcanic ash. Three studies focused on cytotoxicity using samples from the 18 May 1980 Mount St. Helens eruption, USA (Martin et al., 1984) and the 1995-2013 Soufrière Hills eruption, Montserrat (Cullen et al., 2002; Wilson et al., 2000), and only one study also assessed the pro-inflammatory response of these cells (IL-6, IL-8 and IL-1β release) using samples from 6 different volcanic eruptions with variable content of crystalline silica (Damby et al., 2016). All of these studies reported little cytotoxicity of volcanic ash, irrespective of the sample, in agreement with our results. Using doses of respirable ash between 5 and 50 μg/cm^2, and a 24 h timepoint, Damby et al. (2016) showed that IL-1β is not produced by A549 cells, even following quartz treatment. We observe the same in our experiments, even at a higher dose (105 μg/cm^2). The release of IL-6 and IL-8 observed here after 24 h (Fig. 7c) is not reported by Damby et al. (2016), IL-8 not being even produced by quartz treatment in their experiments. These contrasting results could be explained by the difference in particle doses (maximum of 50 μg/cm^2 in Damby et al. (2016) vs. 105 μg/cm^2 here). The relevance of this difference in maximum dose is unknown given a lack of available *in-vivo* dosimetric data during volcanic eruptions (Tomašek et al., 2016), particularly in the context of the Tungurahua area, given the long exposure duration, spatial variations in the characteristics of volcanic ash deposits and environmental conditions, and disparities in human activity. Regardless, our work demonstrates that respirable volcanic ash from the 16-17 August 2006 paroxysmal phase of Tungurahua can initiate a low-level pro-inflammatory response in A549 cells, even when not containing crystalline silica. This work also shows that the alveolar epithelium has a weak inflammatory role but could rather have a signaling role in order to initiate the recruitment of macrophages and the on-set of a global inflammation status.

In the context of the long exposure duration of the populations in the Tungurahua region, these different findings provide justification for dedicated exposure and epidemiological studies. After the first year of activity, increased respiratory infections were reported in Penipe, a town just south of Puela (Fig. 1), which was exposed to the early ashfalls of the Tungurahua eruption but was not evacuated (Tobin & Whiteford, 2004). Little to no

health data on the populations after 2001 have been published, except for qualitative reports of increased respiratory problems from health care professionals described in Sword-Daniels et al. (2011). Such reports suggest that a long-term, chronic respiratory hazard could exist, which could be further investigated.

5 Conclusions

Outside of life-safety risk assessments, health risk assessments at active volcanoes are exceptionally rare, even at highly hazardous volcanoes like Tungurahua, where frequent ash-forming explosive events occurred for almost two decades, subjecting local populations to chronic volcanic particulate matter (PM) exposure, and to respirable volcanic ash in particular. This study highlights that, in such a context of prolonged volcanic activity, to comprehensively assess the resilience of the Tungurahua social-ecological system, the health risks need to be included. Indeed, this work evidences that large quantities of respirable volcanic ash were produced by the sole 16-17 August 2006 explosive phase, which affected the whole agricultural area surrounding the volcano, where more than 60% of adults are outdoor workers. We show that PDC and co-PDC formations are key eruptive phenomena, probably contributing significantly to the high content of respirable ash from this explosive phase.

This work provides the first mapping of inhalable and respirable volcanic ash around an active volcano, and details systematic and large spatial variability, a critical parameter to consider during respiratory health hazard assessments and interpretations of exposures. These novel results provide grounds for future exposure measurements and air quality monitoring campaigns, particularly targeting outdoor workers. We also emphasize the importance of using the mass per unit area of inhalable volcanic ash deposited for quantifying the respiratory health hazard. During the Tungurahua eruption, the amount of respirable ash as well as their physicochemical properties are dependent on the eruption dynamics (e.g., eruptive phenomena such as formation of PDCs, mechanisms of ash transport and deposition). Quantifying the eruption dynamics is thus of critical importance for improved health hazard assessment.

Overall, the respirable ash sample has a low toxic potential in view of the mineralogical content and the particle morphologies. The *in-vitro* assays on A549 cells, a widely used model for human alveolar epithelial type II cells, demonstrate that respirable volcanic ash is efficiently internalized by the cells and processed in the endosomal pathway. No membrane destabilization was observed, which should be further investigated to

understand the longer-term fate of these particles. Additionally, the acute inflammatory response of these cells evidences the potential for the Tungurahua respirable ash to initiate a low-level inflammatory signal, which could lead to chronic inflammation by recruitment of immune cells. Further research to understand the biological response to a chronic exposure to this volcanic ash would beneficially improve overall understanding.

Acknowledgments

J.E., L.G., V.S. and L.B. acknowledge funding from the University Clermont-Auvergne I-Site CAP20-25 program that supported this work. J.E. thanks Jeanne Tran Van Nhieu and Pascale Gueirard for invaluable insights on the TEM images, and Marilyne Lavergne and Helena Choltus for training and support in the biology laboratory. D.D. acknowledges support from the WOW! Visiting Scholar Fellowship from the University Clermont-Auvergne. We thank Gabriel Filippelli for its editorial handling of this manuscript, as well as Dork Sahagian and one anonymous reviewer for their constructive comments. We also thank Natalia Deligne for her insightful internal USGS review. Any use of trade, firm, or product names is for descriptive purposes only and does not imply endorsement by the U.S. Government. This is Laboratory of Excellence ClerVolc contribution n° 566.

Open Research

The grainsize distributions of the individual tephra fall samples, the grainsize distribution of the respirable ash sample isolated from F2, the Raman point counting data and individual spectra, the SEM images and EDX maps of the respirable ash sample, the SEM and TEM images of the *in-vitro* experiments, and the data from the LDH assays, multiplex immunoassays and RT-qPCR are available at https://zenodo.org/record/7094614#.YyxpwnZBxPb via doi: 10.5281/zenodo.7094614 with open access.

REFERENCES

Armijos, M. T., Phillips, J., Wilkinson, E., Barclay, J., Hicks, A., Palacios, P., . . . Stone, J. (2017). Adapting to changes in volcanic behaviour: Formal and informal interactions for enhanced risk management at Tungurahua Volcano, Ecuador. *Global Environmental Change, 45*, 217-226. doi:https://doi.org/10.1016/j.gloenvcha.2017.06.002

Balsa, A. I., Caffera, M., & Bloomfield, J. (2016). Exposures to Particulate Matter from the Eruptions of the Puyehue Volcano and Birth Outcomes in Montevideo, Uruguay. *Environmental Health Perspectives, 124*(11), 1816-1822. doi:doi:10.1289/EHP235

Barclay, J., Few, R., Armijos, M. T., Phillips, J. C., Pyle, D. M., Hicks, A., . . . Robertson, R. E. A. (2019). Livelihoods, Wellbeing and the Risk to Life During Volcanic Eruptions. *Frontiers in Earth Science, 7*(205). doi:10.3389/feart.2019.00205

Baxter, P. J., Searl, A. S., Cowie, H. A., Jarvis, D., & Horwell, C. J. (2014). Chapter 22 Evaluating the respiratory health risks of volcanic ash at the eruption of the Soufrière Hills Volcano, Montserrat, 1995 to 2010. *Geological Society, London, Memoirs, 39*(1), 407-425. doi:10.1144/m39.22

Bernard, B. (2013). Homemade ashmeter: a low-cost, high-efficiency solution to improve tephra field-data collection for contemporary explosive eruptions. *Journal of Applied Volcanology, 2*(1), 1. doi:10.1186/2191-5040-2-1

Bernard, J., Eychenne, J., Le Pennec, J.-L., & Narváez, D. (2016). Mass budget partitioning during explosive eruptions: insights from the 2006 paroxysm of Tungurahua volcano, Ecuador. *Geochemistry, Geophysics, Geosystems, 17*(8), 3224-3240. doi:10.1002/2016GC006431

Bernard, J., Kelfoun, K., Le Pennec, J.-L., & Vallejo Vargas, S. (2014). Pyroclastic flow erosion and bulking processes: comparing field-based vs. modeling results at Tungurahua volcano, Ecuador. *Bulletin of Volcanology, 76*(9). doi:10.1007/s00445-014-0858-y

Bernard, J., & Le Pennec, J.-L. (2016). The milling factory: Componentry-dependent fragmentation and fines production in pyroclastic flows. *Geology, 44*(11), 907-910. doi:10.1130/G38198.1

Bonadonna, C., Ernst, G. G. J., & Sparks, R. S. J. (1998). Thickness variations and volume estimates of tephra fall deposits: the importance of particle Reynolds number. *Journal of Volcanology and Geothermal Research, 81*(3-4), 173-187.

Bonadonna, C., Mayberry, G. C., Calder, E. S., Sparks, R. S. J., Choux, C., Jackson, P., . . . Young, S. R. (2002). Tephra fallout in the eruption of Soufriere Hills Volcano, Montserrat. *Geological Society, London, Memoirs, 21*(1), 483-516. doi:10.1144/gsl.mem.2002.021.01.22

Brown, J. S., Gordon, T., Price, O., & Asgharian, B. (2013). Thoracic and respirable particle definitions for human health risk assessment. *Particle and Fibre Toxicology, 10*, 12-12. doi:10.1186/1743-8977-10-12

Buckland, H. M., Eychenne, J., Rust, A. C., & Cashman, K. V. (2018). Relating the physical properties of volcanic rocks to the characteristics of ash generated by experimental abrasion. *Journal of Volcanology and Geothermal Research, 349*(Supplement C), 335-350. doi:https://doi.org/10.1016/j.jvolgeores.2017.11.017

Bustillos, J., Romero, J. E., Troncoso, L., & Guevara, A. (2016). Tephra fall at Tungurahua Volcano (Ecuador) - 1999-2014: An Example of Tephra Accumulation from a Long-lasting Eruptive Cycle. *Geofis. Intl., 55*(1), 55-67.

Bustin, S. A., Benes, V., Garson, J. A., Hellemans, J., Huggett, J., Kubista, M., . . . Wittwer, C. T. (2009). The MIQE Guidelines: Minimum Information for Publication of Quantitative Real-Time PCR Experiments. *Clinical Chemistry, 55*(4), 611-622. doi:10.1373/clinchem.2008.112797

Carlsen, H. K., Gislason, T., Forsberg, B., Meister, K., Thorsteinsson, T., Jóhannsson, T., . . . Oudin, A. (2015). Emergency hospital visits in association with volcanic ash, dust storms and other sources of ambient particles: a time-series study in Reykjavík, Iceland. *International journal of environmental research and public health, 12*(4), 4047-4059.

Cashman, K., & Rust, A. (2016). Volcanic ash – generation and spatial variations In S. Mackie, H. Ricketts, M. Watson, K. Cashman, & A. Rust (Eds.), *Volcanic ash: hazard observation*: Elsevier.

Cullen, R., Jones, A., Miller, B., Tran, C., Davis, J., Donaldson, K., . . . Morgan, A. (2002). *Toxicity of volcanic ash from Montserrat*: Institute of Occupational Medicine Edinburgh.

Cutler, N. A., Shears, O. M., Streeter, R. T., & Dugmore, A. J. (2016). Impact of small-scale vegetation structure on tephra layer preservation. Scientific Reports, 6(1), 37260. doi:10.1038/srep37260

Damby, D. E. (2012). *From Dome to Disease: The respiratory toxicity of volcanic cristobalite.* (PhD), Durham University, Durham. (7328)

Damby, D. E., Horwell, C. J., Baxter, P. J., Delmelle, P., Donaldson, K., Dunster, C., . . . Tomatis, M. (2013). The respiratory health hazard of tephra from the 2010 Centennial eruption of Merapi with implications for occupational mining of deposits. *Journal of Volcanology and Geothermal Research, 261*, 376-387. doi:https://doi.org/10.1016/j.jvolgeores.2012.09.001

Damby, D. E., Horwell, C. J., Baxter, P. J., Kueppers, U., Schnurr, M., Dingwell, D. B., & Duewell, P. (2018). Volcanic Ash Activates the NLRP3 Inflammasome in Murine and Human Macrophages. *Frontiers in Immunology, 8*(2000). doi:10.3389/fimmu.2017.02000

Damby, D. E., Horwell, C. J., Larsen, G., Thordarson, T., Tomatis, M., Fubini, B., & Donaldson, K. (2017). Assessment of the potential respiratory hazard of volcanic ash from future Icelandic eruptions: a study of archived basaltic to rhyolitic ash samples. *Environmental Health, 16*(1), 98. doi:10.1186/s12940-017-0302-9

Damby, D. E., Llewellin, E. W., Horwell, C. J., Williamson, B. J., Najorka, J., Cressey, G., & Carpenter, M. (2014). The [alpha]-[beta] phase transition in volcanic cristobalite. *Journal of Applied Crystallography, 47*(4), 1205-1215. doi:doi:10.1107/S160057671401070X

Damby, D. E., Murphy, F. A., Horwell, C. J., Raftis, J., & Donaldson, K. (2016). The in vitro respiratory toxicity of cristobalite-bearing volcanic ash. *Environmental Research, 145*, 74-84.

Delmelle, P., Lambert, M., Dufrêne, Y., Gerin, P., & Óskarsson, N. (2007). Gas/aerosol–ash interaction in volcanic plumes: New insights from surface analyses of fine ash particles. *Earth and Planetary Science Letters, 259*(1), 159-170. doi:https://doi.org/10.1016/j.epsl.2007.04.052

Engwell, S., & Eychenne, J. (2016). Chapter 4 - Contribution of Fine Ash to the Atmosphere From Plumes Associated With Pyroclastic Density Currents A2 - Mackie, Shona. In K. Cashman, H. Ricketts, A. Rust, & M. Watson (Eds.), *Volcanic Ash* (pp. 67-85): Elsevier.

Eychenne, J., Cashman, K. V., Rust, A. C., & Durant, A. (2015). Impact of the lateral blast on the spatial pattern and grain size characteristics of the May 18, 1980 Mount St. Helens fallout deposit. *Journal of Geophysical Research, 120*, 6018-6038.

Eychenne, J., & Engwell, S. (2022). The grainsize of volcanic fall deposits: spatial trends and physical controls. *Geological Society of America Bulletin*.

Eychenne, J., Le Pennec, J.-L., Ramón, P., & Yepes, H. (2013). Dynamics of explosive paroxysms at open-vent andesitic systems: High-resolution mass distribution analyses of the 2006 Tungurahua fall deposit (Ecuador). *Earth and Planetary Science Letters, 361*, 343-355. doi:10.1016/j.epsl.2012.11.002

Eychenne, J., Le Pennec, J.-L., Troncoso, L., Gouhier, M., & Nedelec, J.-M. (2012). Causes and consequences of bimodal grain-size distribution of tephra fall deposited during the August 2006 Tungurahua eruption (Ecuador). *Bulletin of Volcanology, 74*(1), 187-205. doi:10.1007/s00445-011-0517-5

Few, R., Armijos, M. T., & Barclay, J. (2017). Living with Volcan Tungurahua: The dynamics of vulnerability during prolonged volcanic activity. *Geoforum, 80*, 72-81. doi:https://doi.org/10.1016/j.geoforum.2017.01.006

Fisher, R. (1964). Maximum Size, Median Diameter, and Sorting of Tephra. *Journal of Geophysical Research, 69*, 341-355.

Forte, P., Domínguez, L., Bonadonna, C., Gregg, C. E., Bran, D., Bird, D., & Castro, J. M. (2018). Ash resuspension related to the 2011–2012 Cordón Caulle eruption, Chile, in a rural community of Patagonia, Argentina. *Journal of Volcanology and Geothermal Research, 350*, 18-32. doi:https://doi.org/10.1016/j.jvolgeores.2017.11.021

Freire, S., Florczyk, A. J., Pesaresi, M., & Sliuzas, R. (2019). An Improved Global Analysis of Population Distribution in Proximity to Active Volcanoes, 1975–2015. *ISPRS International Journal of Geo-Information, 8*(8), 341.

Frezzotti, M. L., Tecce, F., & Casagli, A. (2012). Raman spectroscopy for fluid inclusion analysis. *Journal of Geochemical Exploration, 112*, 1-20. doi:https://doi.org/10.1016/j.gexplo.2011.09.009

Geys, J., Nemery, B., & Hoet, P. H. M. (2010). Assay conditions can influence the outcome of cytotoxicity tests of nanomaterials: Better assay characterization is needed to compare studies. *Toxicology in Vitro, 24*(2), 620-629. doi:https://doi.org/10.1016/j.tiv.2009.10.007

Green, F. H., Vallyathan, V., Mentnech, M. S., Tucker, J. H., Merchant, J. A., Kiessling, P. J., . . . Parshley, P. (1981). Is volcanic ash a pneumoconiosis risk? *Nature, 293*(5829), 216.

Grytting, V. S., Refsnes, M., Låg, M., Erichsen, E., Røhr, T. S., Snilsberg, B., . . . Øvrevik, J. (2022). The importance of mineralogical composition for the cytotoxic and pro-inflammatory effects of mineral dust. *Particle and Fibre Toxicology, 19*(1), 46. doi:10.1186/s12989-022-00486-7

Guimarães, L. F., Nieto-Torres, A., Bonadonna, C., & Frischknecht, C. (2021). A New Inclusive Volcanic Risk Ranking, Part 2: Application to Latin America. *Frontiers in Earth Science, 9*(936). doi:10.3389/feart.2021.757742

Hadley, D., Hufford, G. L., & Simpson, J. J. (2004). Resuspension of Relic Volcanic Ash and Dust from Katmai: Still an Aviation Hazard. *Weather and Forecasting, 19*(5), 829-840. doi:10.1175/1520-0434(2004)019<0829:RORVAA>2.0.CO;2

Hendrix, D. A., Hurowitz, J. A., Glotch, T. D., & Schoonen, M. A. A. (2021). Olivine Dissolution in Simulated Lung and Gastric Fluid as an Analog to the Behavior of Lunar Particulate Matter Inside the Human Respiratory and Gastrointestinal Systems. *GeoHealth, 5*(11), e2021GH000491. doi:https://doi.org/10.1029/2021GH000491

Hendrix, D. A., Port, S. T., Hurowitz, J. A., & Schoonen, M. A. (2019). Measurement of OH* Generation by Pulverized Minerals Using Electron Spin Resonance Spectroscopy and Implications for the Reactivity of Planetary Regolith. *GeoHealth, 3*(1), 28-42. doi: https://doi.org/10.1029/2018GH000175

Hidalgo, S., Battaglia, J., Arellano, S., Steele, A., Bernard, B., Bourquin, J., . . . Vásconez, F. (2015). SO2 degassing at Tungurahua volcano (Ecuador) between 2007 and 2013: Transition from continuous to episodic activity. *Journal of Volcanology and Geothermal Research, 298*(0), 1-14. doi:http://dx.doi.org/10.1016/j.jvolgeores.2015.03.022

Hornby, A., Kueppers, U., Maurer, B., Poetsch, C., & Dingwell, D. (2020). Experimental constraints on volcanic ash generation and clast morphometrics in pyroclastic density currents and granular flows. *Volcanica, 3*(2), 263-283. doi:10.30909/vol.03.02.263283

Horwell, C. (2007). Grain-size analysis of volcanic ash for the rapid assessment of respiratory health hazard. *Journal of Environmental Monitoring, 9*, 1107-1115. doi:10.1039/b710583p

Horwell, C., & Baxter, P. (2006). The respiratory health hazards of volcanic ash: a review for volcanic risk mitigation. *Bull Volcanol, 69*, 1 - 24.

Horwell, C., Fenoglio, I., Ragnarsdottir, K., Sparks, R., & Fubini, B. (2003). Surface reactivity of volcanic ash from the eruption of Soufriere Hills volcano, Montserrat, West Indies with implications for health hazards. *Environ Res, 93*, 202 - 215.

Horwell, C. J., Baxter, P. J., Hillman, S. E., Calkins, J. A., Damby, D. E., Delmelle, P., . . . Tomatis, M. (2013). Physicochemical and toxicological profiling of ash from the 2010 and 2011 eruptions of Eyjafjallajökull and Grímsvötn volcanoes, Iceland using a rapid respiratory hazard assessment protocol. *Environmental Research, 127*, 63-73. doi:https://doi.org/10.1016/j.envres.2013.08.011

IARC. (2012). Arsenic, Metals, Fibres and Dusts. A review of human carcinogens. *IARC Monographs on the Evaluation of Carcinogenic Risks to Humans, World Health Organization, 100C*. doi:PMID:18335640

Institute, H. E. (2020). *State of Global Air 2020*. Retrieved from Boston, MA: https://www.stateofglobalair.org/

Jarvis, P. A., Bonadonna, C., Dominguez, L., Forte, P., Frischknecht, C., Bran, D., . . . Wallace, K. L. (2020). Aeolian Remobilisation of Volcanic Ash: Outcomes of a Workshop in the Argentinian Patagonia. *Frontiers in Earth Science, 8*. doi:10.3389/feart.2020.575184

Le Pennec, J.-L., Ruiz, G. A., Ramón, P., Palacios, E., Mothes, P., & Yepes, H. (2012). Impact of tephra falls on Andean communities: The influences of eruption size and weather conditions during the 1999–2001 activity of Tungurahua volcano, Ecuador. *Journal of Volcanology and Geothermal Research, 217-218*, 91-103. doi:10.1016/j.jvolgeores.2011.06.011

Lee, S. H., & Richards, R. J. (2004). Montserrat volcanic ash induces lymph node granuloma and delayed lung inflammation. *Toxicology, 195*(2-3), 155-165.

Leibrandt, S., & Le Pennec, J.-L. (2015). Towards fast and routine analyses of volcanic ash morphometry for eruption surveillance applications. *Journal of Volcanology and Geothermal Research, 297*(0), 11-27. doi:http://dx.doi.org/10.1016/j.jvolgeores.2015.03.014

Martin, T. R., Ayars, G., Butler, J., & Altman, L. C. (1984). The comparative toxicity of volcanic ash and quartz: effects on cells derived from the human lung. *American Review of Respiratory Disease, 130*(5), 778-782.

Monick, M. M., Baltrusaitis, J., Powers, L. S., Borcherding, J. A., Caraballo, J. C., Mudunkotuwa, I., . . . Grassian, V. H. (2013). Effects of Eyjafjallajökull volcanic ash on innate immune system responses and bacterial growth in vitro. *Environmental Health Perspectives, 121*(6), 691-698.

Mothes, P. A., Yepes, H. A., Hall, M. L., Ramón, P. A., Steele, A. L., & Ruiz, M. C. (2015). The scientific–community interface over the fifteen-year eruptive episode of Tungurahua Volcano, Ecuador. *Journal of Applied Volcanology, 4*(1), 9. doi:10.1186/s13617-015-0025-y

Moune, S., Gauthier, P.-J., & Delmelle, P. (2010). Trace elements in the particulate phase of the plume of Masaya Volcano, Nicaragua. *Journal of Volcanology and Geothermal Research, 193*(3), 232-244. doi:https://doi.org/10.1016/j.jvolgeores.2010.04.004

Muller, C., Biggs, J., Ebmeier, S. K., Mothes, P., Palacios, P. B., Jarrín, P., . . . Ruiz, M. (2018). Temporal evolution of the magmatic system at Tungurahua Volcano, Ecuador, detected by geodetic observations. *Journal of Volcanology and Geothermal Research, 368*, 63-72. doi:https://doi.org/10.1016/j.jvolgeores.2018.11.004

Pavan, C., Sydor, M. J., Bellomo, C., Leinardi, R., Cananà, S., Kendall, R. L., . . . Turci, F. (2022). Molecular recognition between membrane epitopes and nearly free surface silanols explains silica membranolytic activity. *Colloids and Surfaces B: Biointerfaces, 217*, 112625. doi:https://doi.org/10.1016/j.colsurfb.2022.112625

Samaniego, P., Le Pennec, J.-L., Robin, C., & Hidalgo, S. (2011). Petrological analysis of the pre-eruptive magmatic process prior to the 2006 explosive eruptions at Tungurahua volcano (Ecuador). *Journal of Volcanology and Geothermal Research, 199*(1-2), 69-84.

Sauzéat, L., Eychenne, J., Gurioli, L., Boyet, M., Jessop, D., Moretti, R., . . . Volle, D. H. (2022). Metallome deregulation and health-related impacts due to long-term exposure to recent volcanic ash deposits: New chemical and isotopic insights. *Science of The Total Environment*, 154383. doi:https://doi.org/10.1016/j.scitotenv.2022.154383

Sauzéat, L., Bernard, E., Perret-Liaudet, A., Quadrio, I., Vighetto, A., Krolak-Salmon, P., . . . Balter, V. (2018). Isotopic Evidence for Disrupted Copper Metabolism in Amyotrophic Lateral Sclerosis. *iScience, 6*, 264-271. doi:https://doi.org/10.1016/j.isci.2018.07.023

Schiavi, F., Bolfan-Casanova, N., Withers, A. C., Médard, E., Laumonier, M., Laporte, D., . . . Gómez-Ulla, A. (2018). Water quantification in silicate glasses by Raman spectroscopy: Correcting for the effects of confocality, density and ferric iron. *Chemical Geology, 483*, 312-331. doi:https://doi.org/10.1016/j.chemgeo.2018.02.036

Searl, A., Nicholl, A., & Baxter, P. J. (2002). Assessment of the exposure of islanders to ash from the Soufriere Hills volcano, Montserrat, British West Indies. *Occupational and Environmental Medicine, 59*(8), 523. doi:10.1136/oem.59.8.523

Stewart, C., Damby, D. E., Horwell, C. J., Elias, T., Ilyinskaya, E., Tomašek, I., . . . Witham, C. (2022). Volcanic air pollution and human health: recent advances and future directions. *Bulletin of Volcanology, 84*(1), 11. doi:10.1007/s00445-021-01513-9

Stone, J., Barclay, J., Simmons, P., Cole, P. D., Loughlin, S. C., Ramón, P., & Mothes, P. (2014). Risk reduction through community-based monitoring: the vigías of Tungurahua, Ecuador. *Journal of Applied Volcanology, 3*(1), 11. doi:10.1186/s13617-014-0011-9

Sword-Daniels, V., Wardman, J., Stewart, C., Wilson, T. M., Johnston, D. M., & Rossetto, T. (2011). *Infrastructure impacts, management and adaptations to eruptions at Volcán Tungurahua, Ecuador, 1999-2010*. Retrieved from

Thorsteinsson, T., Jóhannsson, T., Stohl, A., & Kristiansen, N. I. (2012). High levels of particulate matter in Iceland due to direct ash emissions by the Eyjafjallajökull eruption and resuspension of deposited ash. *Journal of Geophysical Research: Solid Earth, 117*(B9). doi:10.1029/2011jb008756

Tobin, G. A., & Whiteford, L. M. (2002). Community Resilience and Volcano Hazard: The Eruption of Tungurahua and Evacuation of the Faldas in Ecuador. *Disasters, 26*(1), 28-48. doi:10.1111/1467-7717.00189

Tobin, G. A., & Whiteford, L. M. (2004). *Chronic hazards: Health impacts associated with on-going ash-falls around Mt. Tungurahua in Ecuador.* Paper presented at the Applied Geography Conferences.

Tomašek, I., Damby, D. E., Andronico, D., Baxter, P. J., Boonen, I., Claeys, P., . . . Elskens, M. (2021a). Assessing the biological reactivity of organic compounds on volcanic ash: implications for human health hazard. *Bulletin of Volcanology, 83*(5), 30. doi:10.1007/s00445-021-01453-4

Tomašek, I., Damby, D. E., Stewart, C., Horwell, C. J., Plumlee, G., Ottley, C. J., . . . Leermakers, M. (2021b). Development of a simulated lung fluid leaching method to assess the release of potentially toxic elements from volcanic ash. *Chemosphere, 278*, 130303. doi:https://doi.org/10.1016/j.chemosphere.2021.130303

Tomašek, I., Horwell, C. J., Damby, D. E., Barošová, H., Geers, C., Petri-Fink, A., . . . Clift, M. J. D. (2016). Combined exposure of diesel exhaust particles and respirable Soufrière Hills volcanic ash causes a (pro-)inflammatory response in an in vitro multicellular epithelial tissue barrier model. *Particle and Fibre Toxicology, 13*(1), 67. doi:10.1186/s12989-016-0178-9

Wadge, G., Voight, B., Sparks, R. S. J., Cole, P. D., Loughlin, S. C., & Robertson, R. E. A. (2014). Chapter 1 An overview of the eruption of Soufrière Hills Volcano, Montserrat from 2000 to 2010. *Geological Society, London, Memoirs, 39*(1), 1. doi:10.1144/M39.1

Whiteford, L. M., & Tobin, G. A. (2004). Saving lives, destroying livelihoods: emergency evacuation and resettlement policies in Ecuador. *Unhealthy health policy: a critical anthropological examination, 189*, 202.

Wilson, M. R., Stone, V., Cullen, R. T., Searl, A., Maynard, R. L., & Donaldson, K. (2000). In vitro toxicology of respirable Montserrat volcanic ash. *Occupational and Environmental Medicine, 57*(11), 727-733.

Wright, H. M. N., Cashman, K., Mothes, P. A., Hall, M. L., Ruiz, G. A., & Le Pennec, J. L. (2012). Estimating rates of decompression from textures of erupted ash particles produced by 1999–2006 eruptions of Tungurahua volcano, Ecuador. *Geology, 40*(7), 619-622.

Tables

Human Gene	Sequence (5'→3')	Product length (bp)	Annealing temperature (°C)
hIL1β-F	AATCTCCGACCACCACTACAG	174	62
hIL1β-R	TCCCATGTGTCGAAGAAGATAG		
hIL6-F	AATGAGGAGACTTGCCTGGTG	143	61
hIL6-R	AGGAACTGGATCAGGACTTTTG		
hIL8-F	GATTTCTGCAGCTCTGTGTG	154	61
hIL8-R	TCTGTGTTGGCGCAGTGTGG		
hTNFα-F	AGGGACCTCTCTCTAATCAGC	168	61
hTNFα-R	TCTCAGCTCCACGCCATTGG		
hRPLP0-F	AGGCTTTAGGTATCACCACT	219	61
hRPLP0-R	GCAGAGTTTCCTCTGTGATA		
hRPS17-F	TGCGAGGAGATCGCCATTATC	170	61
hRPS17-R	AAGGCTGAGACCTCAGGAAC		

Table 1: Forward (-F) and reverse (-R) primer sequences used for RT-qPCR amplification of human genes.

Sample	UTM coordinates (zone 17, hemisphere S) E	N	Dist. from vent (km)	Total MpUA (kg/m²)	wt.% < 63 µm	< 10 µm	< 4 µm	< 2.5 µm	< 1 µm	MpUA (kg/m²) < 63 µm	< 10 µm	< 4 µm	< 2.5 µm	< 1 µm
F 1	776681	9841976	8.5 NW	29.1	14.4	3.7	1.5	1.1	0.4	4.2	1.1	0.4	0.3	0.1
F 2 *	776416	9839600	7.9 WNW	100.2	38.8	11.9	5.3	4.1	1.9	38.9	12.0	5.3	4.1	1.9
F 3	768261	9849616	20.6 NW	2.7	5.9	1.5	0.6	0.5	0.3	0.2	0.04	0.02	0.01	0.01
F 4	767139	9843956	18.1 WNW	10.3	24.2	6.2	3.0	2.4	1.3	2.5	0.6	0.3	0.2	0.1
F 5	771469	9839734	12.8 W	37.2	32.3	9.6	4.6	3.7	2.1	12.0	3.6	1.7	1.4	0.8
F 6	770323	9838700	13.9 W	27.0	31.7	9.3	4.5	3.6	2.0	8.6	2.5	1.2	1.0	0.5
F 7	769701	9841314	14.9 WNW	25.9	33.9	10.5	5.1	4.1	2.1	8.8	2.7	1.3	1.1	0.5
F 8	766408	9848198	20.6 NW	6.3	21.2	5.2	2.2	1.8	0.8	1.3	0.3	0.1	0.1	0.05
F 9	765393	9838940	18.8 W	14.4	29.0	8.3	4.1	3.4	1.8	4.2	1.2	0.6	0.5	0.3
F 10	765203	9843728	19.9 WNW	6.7	23.1	7.6	3.7	2.9	1.5	1.5	0.5	0.2	0.2	0.1
F 11	766895	9841782	17.7 WNW	13.8	29.9	10.1	4.9	3.9	2.0	4.1	1.4	0.7	0.5	0.3
F 12	768190	9841254	16.3 WNW	20.0	33.7	10.3	5.0	4.1	2.2	6.8	2.1	1.0	0.8	0.4
F 13	775412	9837718	8.8 W	63.5	37.7	11.8	5.9	4.8	2.4	24.0	7.5	3.8	3.0	1.5
F 14	769533	9837938	14.7 W	22.4	29.7	9.1	4.3	3.4	1.8	6.7	2.0	1.0	0.8	0.4
F 15	766750	9835702	17.6 W	7.8	22.1	6.5	2.8	2.2	1.2	1.7	0.5	0.2	0.2	0.1
F 16	770009	9834660	14.6 WSW	13.4	15.5	4.1	1.9	1.5	0.8	2.1	0.5	0.3	0.2	0.1
F 17	768594	9833600	16.2 WSW	7.0	19.1	5.6	2.5	2.0	1.0	1.3	0.4	0.2	0.1	0.1
F 18	767830	9832468	17.3 WSW	5.0	18.8	4.3	1.9	1.5	0.8	0.9	0.2	0.1	0.1	0.04
F 19	770958	9833310	14.1 WSW	9.3	11.2	3.1	1.4	1.2	0.6	1.0	0.3	0.1	0.1	0.1
F 20	773566	9833020	11.7 WSW	15.4	10.9	2.7	1.3	1.0	0.5	1.7	0.4	0.2	0.2	0.1
F 21	771414	9835712	12.9 W	17.0	16.7	4.6	2.2	1.8	0.9	2.8	0.8	0.4	0.3	0.2
F 22	773510	9835168	11.0 W	23.9	12.3	3.1	1.5	1.2	0.6	2.9	0.7	0.4	0.3	0.2

Table 2: Sample list, coordinates (WGS 84 map datum), and sedimentological characteristics (including proportions and mass per unit area (MpUA) of the inhalable volcanic ash fractions). Sample locations in Fig. 3. Total MpUA data from Eychenne et al. (2012). * Sample F2 used for aerodynamic separation of the sub-10 µm ash fraction, subsequently used for physicochemical characterisation and biological *in-vitro* experiments.

Phases		nb%	Standard chemical compositions
Feldspars	Plagioclase	42	$Na(AlSi_3O_8)$ - $Ca(Al_2Si_2O_8)$
	Sanidine		$K(AlSi_3O_8)$
Glasses	Andesitic	23	61.2 ± 0.6 wt.% SiO_2 *
	Rhyolitic		71.6 ± 2.5 wt.% SiO_2 *
Clinopyroxenes	Augite	11	$(Ca,Na)(Mg,Fe,Al,Ti)(Si,Al)_2O_6$
	Pigeonite		$(Ca,Mg,Fe)(Mg,Fe)Si_2O_6$
Orthopyroxene	Hypersthene	1	$(Mg,Fe)SiO_3$
Anatase		6	TiO_2
Magnetite		9	$Fe^{2+}Fe^{3+}{}_2O_4$
Hematite		7	Fe_2O_3
Alunite		1	$KAl_3(SO_4)_2(OH)_6$
Rutile		-	TiO_2
Olivine		-	$(Mg,Fe)_2SiO_4$
Carbonaceous matter		-	C-C and C-H bonds

Table 3: Mineralogical phases and grain number proportions (nb%) determined by Raman spectroscopy in the respirable volcanic ash sample from the August 2006 Tungurahua eruption. Standard chemical compositions of each identified phase are given for reference. * Glass compositions inferred from microprobe analyses on lapilli from the same eruption in Samaniego et al. (2011).

Figure captions

Fig. 1: (a) Location map of Ecuador and Tungurahua volcano in the Andean Cordillera (grey shaded area). **(b)** Agricultural area around Tungurahua volcano (red triangle), and locations where the fallout deposit of the 16-17 August 2006 eruptive phase was sampled. The lines of equal deposited mass of particles per unit area during this phase are mapped (white lines) and represent the spatial variations of the amount of particles on the ground. The land in the area is farmed (white transparent area) to the middle of the slope of the Tungurahua volcanic edifice (see also the photograph in Fig. 2a). Location of photograph in Fig. 2b is reported by a yellow star. Base-map layer from Google maps. **(c)** Chronology of the 1999-2016 Tungurahua eruption showing the duration of each explosive eruptive phase and the main changes in intensity (black vs. grey eruptive phases) and steadiness (orange vs. yellow time periods) of the overall activity. Note that the term "eruption" refers to the whole 1999-2016 eruptive period, while "phase" corresponds to the shorter, alternating periods of variably intense explosive activity within the whole duration of the 1999-2016 eruption. Each high (black slots) and low (grey slots) intensity eruptive phase was characterized by explosive plumes reaching an altitude of at least 1 km above the vent and depositing particles in the area defined in **(b)**. After Hidalgo et al. (2015) and Muller et al. (2018).

Fig. 2: (a) Western slope of Tungurahua volcano in September 2019 showing how high the farmed land spreads on the volcano's flank. Photograph by J. Eychenne taken from location F1 on Fig. 1b. **(b)** Greenhouses and crops covered and destroyed by ash from the explosive plume from the 16-17 August 2006 eruptive phase. Photograph by J.-L. Le Pennec, taken one month after this event. See location on Fig. 1b.

Fig. 3: Variations of the inhalable ash fractions across the 16-17 August 2006 Tungurahua fallout deposit. **(a-b)** Decay of deposited sub-10 μm, sub-4 μm, sub-2.5 μm and sub-1 μm volcanic ash with distance from the volcano crater (red triangle on maps; **d-g**) presented as **(a)** mass proportions and **(b)** mass per unit area. Closed and open symbols represent sampled locations on and off the depositional axis, respectively. Colour-shaded areas highlight the on-axis trends. Dashed lines on **(b)** represent the off-axis trends. **(c)** Mass per unit area variations of the bulk deposit and the particles finer than 63 μm with distance from vent in black (left vertical axis). Mass proportions variations of the particles finer than 63 μm with distance from vent in grey (right vertical axis). Closed and open symbols represent on and off the depositional axis, respectively. The solid lines highlight

the decay in mass per unit area along the depositional axis. **(d-g)** Maps of the spatial distribution of the mass per unit area of sub-10 μm **(d)**, sub-4 μm **(e)**, sub-2.5 μm **(f)** and sub-1 μm ash **(g)** in the agricultural area west of Tungurahua volcano, as of September 2006. Closed and open symbols represent on- and off-axis samples, respectively. The solid black lines represent virtual lines of equal deposition (in kg/m^2) of the considered inhalable fraction (dashed lines extend contours into areas poorly constrained by lack of samples). The white squares are small villages identified in Fig. 1. Coloured star identifies sample used for isolation of respirable ash (sample F2). Base-map layer from Google maps.

Fig. 4: (a) Grainsize distribution and **(b-d)** mineralogical componentry of the isolated respirable volcanic ash sample from the August 2006 Tungurahua eruption. **(b)** Number proportion of phases assessed by discrete Raman spectroscopy analyses on 133 individual grains. **(c-d)** Raman spectra for all the mineralogical and carbonaceous phases identified in the sample (vertical axis is arbitrary unit). Accessory phases rutile, olivine, and carbonaceous matter each comprise less than 1 number % of the sample and are excluded from **(b)**.

Fig. 5: Morphology, texture, and near-surface chemistry of the respirable Tungurahua volcanic ash sample, acquired by FIB-SEM in **(a-e)** SE, **(b-j)** BSE and **(k-n)** EDS modes. AG = andesitic glass; RG = rhyolitic glass; P = plagioclase; Px = pyroxene; Cpx = clinopyroxene; Opx = orthopyroxene; Ox = Fe and Ti oxides; S = Potassium and aluminium sulfates (alunite).

Fig. 6: Interactions between A549 cells and respirable Tungurahua volcanic ash or quartz particles imaged by **(a-l)** FEG-SEM and **(m-x)** TEM. **(a-l)** Morphological changes observed after 6 and 24 hours between untreated A549 cells and cells treated with respirable volcanic ash or Min-U-Sil quartz positive control. Representative images of cells treated with volcanic ash at 250 μg/ml are solely presented here because they offer a better view of the cells and the particles, but no major differences in terms of morphology and surface features are observed between cells treated at 250 and 1000 μg/ml (Fig. S1 in Supplemental Material). Q = quartz particles; V = respirable volcanic ash. **(m-x)** Intracellular changes observed after 6 and 24 hours between untreated A549 cells and cells treated with respirable volcanic ash or Min-U-Sil quartz positive control. Like with the SEM images, no major differences are observed between cells treated with 250 and 1000 μg/ml of volcanic ash (Fig. S2 in Supplemental Material). Green stars indicate

treatment dose of volcanic ash (*250 µg/ml, **1000 µg/ml). White bright spots are due to tears in the ultrathin sections caused by the hardness contrast between the particles and the cells during cutting. A = autophagosomes/autophagolysosomes; C= chromatin; E = endocytosis; LB = lamellar bodies; LV = lysis vacuoles; MB = microvesicular bodies; Mi = mitochondria; N = cell nucleus; Q = quartz particles; V = respirable volcanic ash.

Fig. 7: (a) Cytotoxicity towards A549 cells of the respirable Tungurahua volcanic ash sample at 2 concentrations and the Min-U-Sil quartz positive control after 6 and 24 hours of exposure, measured by LDH activity relative to untreated cells in duplicates (n=2) of 6 independent experiments (N=6). **(b-c)** Pro-inflammatory response measured by cytokine production by A549 cells after 6 and 24 hours of exposure to 2 concentrations of the respirable Tungurahua volcanic ash and the Min-U-Sil quartz positive control. **(b)** Cytokine gene expression by real-time RT-qPCR on duplicates (n=2) of 4 independent experiments (N=4). Gene expression is normalized to the geometric mean of the expression of two housekeeping genes. **(c)** Cytokine production measured in culture supernatants by automated multiplex immunoassays on Ella™ on the pooled duplicates (for n=1) of 6 independent experiments (N=6). Protein production presented as the cytokine concentration normalized to the total protein concentration. Boxplots in **(a)**, **(b)** and **(c)** are Tukey boxplots with the mean represented as a cross and the median as a horizontal line. *$p \leq 0.05$, **$p \leq 0.01$, ***$p \leq 0.001$.

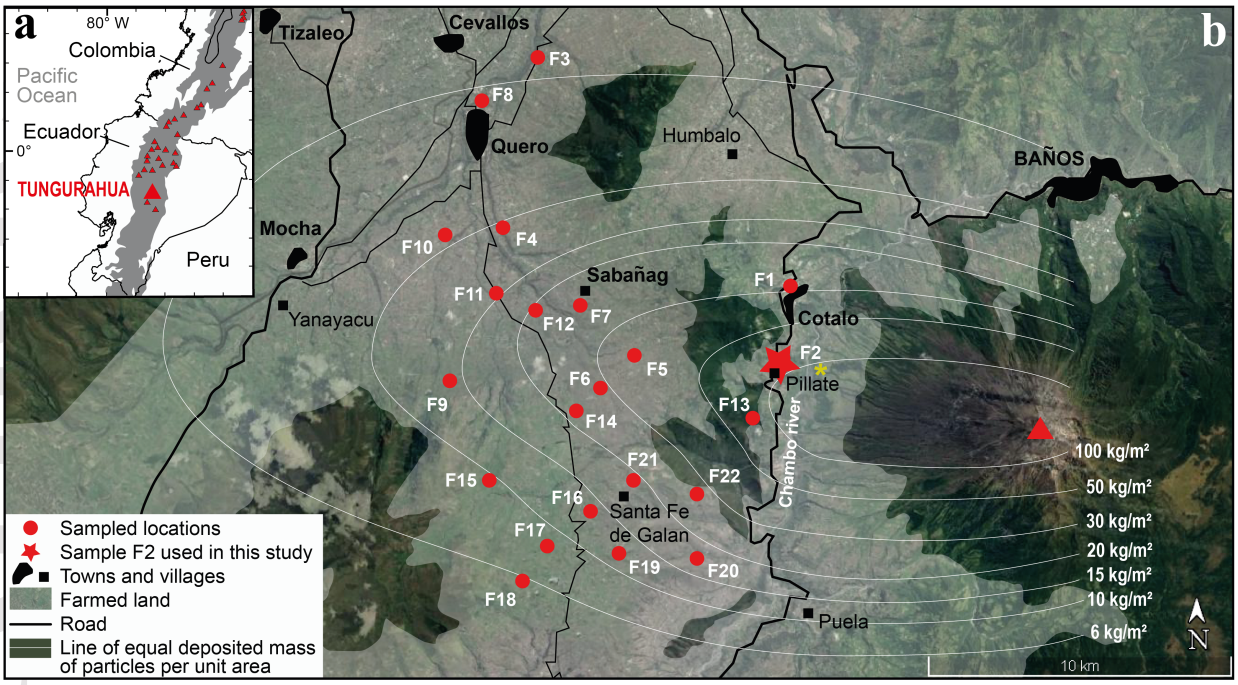

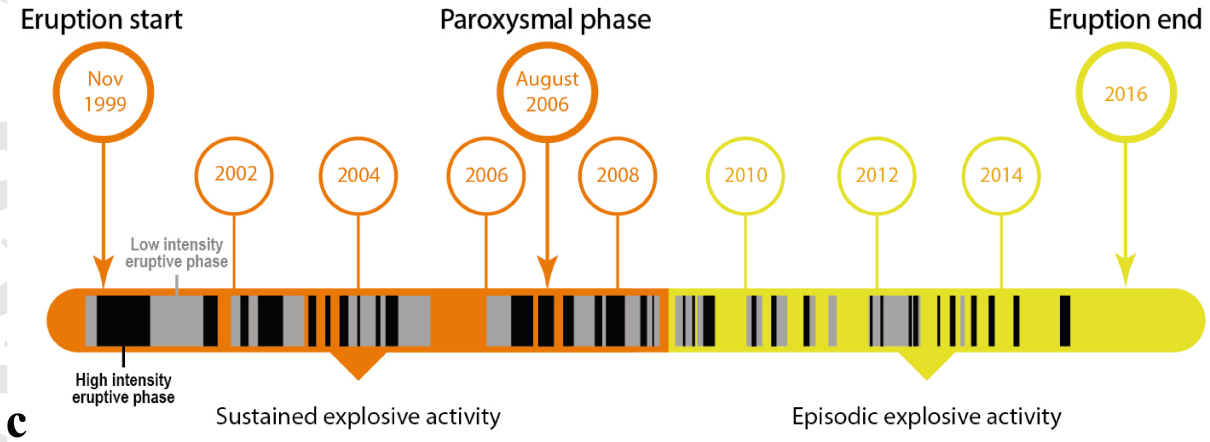

c